Statistical Study of Intrinsic Parasitics in an SPAD-Based Integrated Fiber Optical Receiver

Hiwa Mahmoudi, Michael Hofbauer, Bernhard Steindl, Kerstin Schneider-Hornstein, and Horst Zimmermann, *Senior Member, IEEE*

***Abstract*— Recently, a fully integrated optical fiber receiver was reported based on single-photon avalanche diode detectors to reduce the sensitivity gap to the quantum limit. This was realized through an array of four detectors to overcome the parasitic effects dominated by afterpulsing which prevent a single detector from providing an acceptable performance to serve as an optical receiver. However, the array structure imposes an extra effect called "crosstalk," which needs to be accurately characterized. Thanks to the memoryless nature of dark noise statistics, we present an effective method to investigate the intrinsic parasitic effects of the array based on an all-at-once dark noise measurement. The corresponding detection probabilities and delays versus excess bias voltage are obtained for different parasitics at all detectors. The results are used to model crosstalk and estimate the error probabilities required for bit error ratio analysis and structure optimization. The accuracy of the estimations is verified by experimental data.**

***Index Terms*— Afterpulsing, crosstalk, dark count, detector dead time, optical receiver, single-photon avalanche diode (SPAD).**

I. Introduction

SINGLE-photon avalanche diode (SPAD) is a promising photodetector for optical receivers applications [1]–[4]. An SPAD exhibits a macroscopic current pulse through a self-sustaining avalanche when it is reverse-biased above its breakdown voltage (Geiger mode). Such an avalanche can be triggered by a single charge carrier injected into an active region where a strong electric field accelerates carriers gaining a kinetic energy sufficient for creating electron-hole pairs. Therefore, a single photon absorbed in the active area can be detected by the SPAD and this makes it potentially more sensitive as compared to avalanche photodiodes (APDs), which are biased below breakdown (linear mode) and exhibit limited avalanche multiplication gain [5]–[7]. Nevertheless, nonidealities such as detector blindness during the recovery (dead) time, parasitic effects, limited fill factor, and detection efficiency can significantly degrade the receiver performance [8]. Only recently, it has been shown that a well-designed SPAD-based receiver can bring significant improvements in receiver sensitivity [4], [9]. From a structural point of view, a key tradeoff is between the receiver sensitivity and the minimum achievable bit error ratio (BER), where the former favors a less number of SPADs in the receiver array while the later demands more SPADs to overcome the parasitic effects as will be explained later. Therefore, accurate characterization of the parasitic effects is necessary to model the receiver performance, to estimate the minimum number of SPADs that can provide a desired BER, and to identify the bottleneck for further optimizations.

There have been extensive studies of nonidealities in SPAD-based detectors. For example, the effect of the dead time on photon statistics has been recently comprehensively studied in [10]. However, the model presented in [10] is based on a photon-counting scheme using a single SPAD and the crosstalk effect is not considered. The common method to characterize crosstalk is an SPAD-to-SPAD (one-to-one) crosstalk measurement [11], which requires electrical access to bias individual SPADs. This is not, unfortunately, possible with the array available to the authors (shown in Fig. 1) and usually is not feasible with commercially available SPAD arrays as it adds circuit complexities. Furthermore, selective optical access to individual SPADs needs complicated optical setups [12], [13]. To avoid circuit or optical complications, we present a statistical method based on dark noise statistics, which is the most straightforward case to measure. The presented method is very effective for arrays with SPADs individually connected to a quenching circuit and delivering a processable signal, which is the case for highly sensitive optical receivers [4].

The integrated optical receiver presented in [4] is based on an array of only four SPADs and has paved the way for optical receivers aiming toward the quantum limit. In this paper, we present an experimental investigation and analysis of this SPAD-based integrated optical receiver to characterize its intrinsic parasitic effects, including dark count, afterpulsing, and crosstalk, which are explained in the next section. The implemented characterization methodology regarding these

Manuscript received June 28, 2018; revised October 16, 2018; accepted November 9, 2018. Date of publication December 10, 2018; date of current version December 24, 2018. This work was supported by the Austrian Science Fund (FWF) under Grant P28335-N30. The review of this paper was arranged by Editor J. Huang. *(Corresponding author: Hiwa Mahmoudi.)*

The authors are with the Institute of Electrodynamics, Microwave and Circuit Engineering, Vienna University of Technology, 1040 Vienna, Austria (e-mail: hiwa.mahmoudi@tuwien.ac.at).

Color versions of one or more of the figures in this paper are available online at http://ieeexplore.ieee.org.

Digital Object Identifier 10.1109/TED.2018.2882344

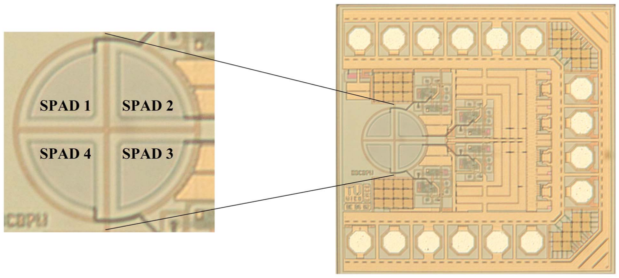

Fig. 1. Microphotograph of the receiver test chip presented in [4].

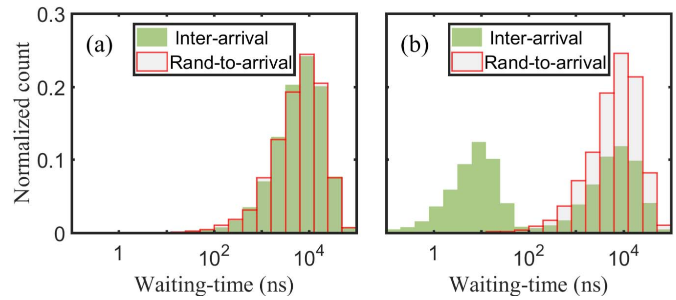

Fig. 2. Waiting-time distribution based on the interarrival and the random-to-arrival schemes for (a) one ($\mathbb{P}\{r_1\}$) and (b) two simultaneous Poisson processes ($\mathbb{P}\{r_1\}$ and $\mathbb{P}\{r_2\}$).

parasitic effects is described in Section III. Then, the investigation results are presented in Section IV where it is shown how the afterpulsing together with the extrinsic parasitics can degrade the BER in a single-SPAD receiver emphasizing the need for multi-SPAD structures. Accordingly, the minimum number of SPADs to achieve a specific BER is discussed, and a crosstalk model is presented, and finally, the conclusion and future work are summarized in Section V.

II. Background and Problem Definition

A. Receiver Structure

Fig. 1 shows a micrograph of the integrated optical receiver presented in [4] based on an array of four SPADs with a diameter of 200 μm and a gap of 34 μm between the SPADs. Each SPAD is connected to an active quenching circuit and a buffer delivers its output signal to a four-channel oscilloscope. The signals are sampled simultaneously and stored by the oscilloscope in 10 blocks for time periods of 2 ms, i.e., a total 20-ms data stream at any given biasing voltage level on the array. Then, the data are imported with 8-bit resolution into MATLAB on a personal computer. More details regarding the receiver chip and the measurement setup are provided in [4].

It is worth mentioning that the chip does not allow for selective access to SPADs as by applying the biasing voltage, the whole array is active. Furthermore, in order to avoid complicated optical setups to provide illumination of individual SPADs, we employ a simple but effective statistical method to study and characterize the intrinsic parasitic effects based on an all-at-once dark noise measurement. In order to obtain dark noise statistics at a given biasing voltage, the receiver was tested at room temperature within a dark box and the detection time corresponding to each SPAD was calculated in MATLAB by comparing the signal to a threshold. Therefore, the obtained data consist of four sequences of successive avalanche detection times in the four SPADs which are recorded simultaneously. Before describing the proposed statistical approach to capture the SPAD parasitic effects, the basic concept behind it is clarified in the next section.

B. Statistical Analysis Principles

The distribution of a random variable (e.g., $\tau = t^* - t_0$ indicating the "waiting time" for the arrival of a certain event at t^*) is memoryless when the distribution depends only on the absolute value of τ and not on the starting point of the interval (i.e., t_0 which indicates the time that has already been passed). In other words, for all $t_0 > 0$ and $\tau_0 > 0$ (τ_0 is a given τ), we have

$$P(\tau > (\tau_0 + t_0) \mid \tau > t_0) = P(\tau > \tau_0). \quad (1)$$

In Fig. 2(a), two histograms represent the distribution of waiting times in a Poisson process ($\mathbb{P}\{r_1\}$), where the interarrival time of the counting process exhibits an exponential distribution which is a memoryless distribution. One histogram corresponds to the interarrival times between 10^5 events which are drawn randomly from an exponential distribution with a rate parameter of $r_1 = 10^5$. Therefore, it is expected that the waiting time has a mean of 10^{-5} s (i.e., 10^4 ns) and the 10^5 successive events form a time sequence with a total length of around 1 s. To inspect the memorylessness, the second histogram characterizes the waiting-time distribution in the same time sequence, but instead of considering the interarrival times, the waiting time is obtained as the time interval between a randomly selected instant in the sequence (t_0) and the first arrival after t_0. According to (1), we expect that both approaches can accurately capture the distribution as it can be seen in Fig. 2(a).

Now, we utilize these approaches to characterize a similar process, but in presence of a second Poisson process (e.g., $\mathbb{P}\{r_2\}$ with a much higher rate of $r_2 = 10^8$) within $\mathbb{P}\{r_1\}$. In fact, if we assume both processes are equally likely and draw 10^5 arrivals to form a time sequence, the interarrival time-based method obtains a waiting-time distribution which includes two exponential distributions as shown in Fig. 2(b). However, if the distribution is evaluated by the random selection-based scheme, the exponential distribution corresponding to $\mathbb{P}\{r_1\}$ is accurately characterized while $\mathbb{P}\{r_2\}$ is completely ignored. Henceforth, this concept will be applied to SPAD experimental dark noise data, which include different noise mechanisms having different rates but with memoryless probabilities.

Fig. 3 shows two histograms regarding the obtained experimental data for SPAD 1, where two (MATLAB) above-mentioned experiments are performed on its acquired time sequence. It is important to note that the widths of the time bins in Fig. 3 are not equal but increase exponentially to allow the observation of dominant avalanche mechanisms in a wide range of nanoseconds to milliseconds. According to the first

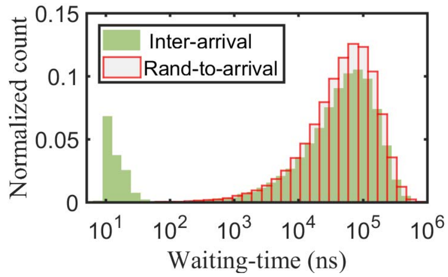

Fig. 3. Waiting-time distribution based on the interarrival and the random-to-arrival schemes. The data are from SPAD 1 at $V_{\text{ex}} \simeq 4$ V.

experiment (interarrival evaluation), there are two dominant avalanche mechanisms, one in the nanosecond range and the other one in the microsecond to millisecond range. The second experiment (random-to-arrival evaluation), however, identifies only the distribution regarding the second mechanism with similar distribution properties specified in the first experiment. This is due to the memoryless nature of the corresponding distribution which is the key property to characterize all parasitic mechanisms as is explained later.

C. Detection Nonidealities and Parasitic Effects

A SPAD operates in the Geiger mode and shows a much higher gain than an APD working in the linear mode and, therefore, eliminates the amplification noise. However, it suffers from other internal parasitic effects, which either make the SPAD blind to the photons or fire an avalanche process without a photon being absorbed. This can significantly influence the SPAD performance as a photodetector and needs to be precisely characterized. In the following, these mechanisms are briefly described.

1) Dead Time: The avalanche process creating the macroscopic current through the SPAD has to be quenched by decreasing the reverse-bias voltage below the breakdown. Then, the bias voltage is restored to above breakdown making the SPAD ready for the next detection. During this quench-reset recovery period which is called “dead time” (t_d), the detector is blind to incident photons. A fast quench-reset action can be accomplished by an active (transistor-based) quenching circuit [14], [15]. The dead time can be estimated as the minimum interarrival time. However, this estimation is limited to the oscilloscope’s time resolution (equal to 2 ns in our experiment) and cannot be more accurate than integer factors of 2 ns. According to Fig. 3, although there are few intervals of 8 ns, the minimum intervals are concentrated on 10 ns. Using a more precise estimation method described in the next section, the dead time is obtained to be $\simeq$9 ns.

2) Dark Count: Under dark condition, the SPAD shows a detection rate called the dark-count rate (r_{dc}) triggered by thermally or tunneling generated carriers. r_{dc} is typically in the range of kilohertz to megahertz and increases with the voltage in excess of breakdown which is known as excess bias voltage (V_{ex}). It may be estimated as one over the average time interval between successive detections in the dark condition but this may overestimate r_{dc} if other parasitic effects are not negligible. The avalanche mechanism with the distribution concentrated on the interval 10^3–10^6 ns shown in Fig. 3 is due to the dark-count mechanism.

3) Afterpulsing: Afterpulsing is an avalanche mechanism which is strongly correlated with previous avalanche detections. It is thought to be caused by charge carriers, which are trapped during the previous avalanches and then are released and detected with a delay (i.e., a waiting time of nanosecond scale), when the SPAD is recovered [16]. Recently, it has been shown that afterpulsing cannot be characterized using a universal mathematical model and every individual detector has to be characterized individually [17].

In general, the afterpulsing probability increases with the excess bias voltage and can strongly limit the high-frequency operating range. In Fig. 3, the avalanche mechanism with the distribution concentrated around 10 ns depicts the afterpulsing effect. It is worthwhile to note that in the experiment based on random values of t_0, the afterpulsing cannot be identified. Therefore, the dark count is accurately characterized based on this experiment as is shown in the next section.

4) Crosstalk: The use of multidetector structures imposes interaction between the SPADs which can be a major concern when they are closely spaced. The crosstalk can be triggered optically by photons emitted from hot carriers in another SPAD where an avalanche has been fired or electrically through diffusing carrier form a neighboring SPAD or through a combination of optical and electrical crosstalk [18], [19].

A high crosstalk probability can significantly degrade the performance of an optical receiver in any frequency regime. In addition, it shows time delays in the nanosecond range close to that of afterpulsing and it may limit the high-frequency operating capability. Therefore, its characterization is crucial, but also tricky, especially when the calibration method based on the one-to-one evaluation is not applicable due to the lack of selective access to bias or illumination of individual SPADs. To effectively address this problem, the next section presents a statistical method based on a simple but meaningful property of the dark noise statistics.

III. Characterization Methodology

Based on a dark measurement at a given biasing condition, we obtain four sequences of successive avalanche detection times for the SPADs in the receiver array, similar to what is shown in Fig. 3. Such sequences contain avalanches generated by all intrinsic parasitic effects including dark count, afterpulsing, and crosstalk. Their characterization means to obtain the expected time delays (i.e., waiting times) as well as their probabilities which is conducted as is described in the following.

A. Dark-Count Measurement

It is well known that the dark-count process shows an exponential distribution [20] which is a memoryless distribution. This means that the waiting time to detect an avalanche due to a dark count is a random value, which does not depend on how much time has passed since the previous avalanche.

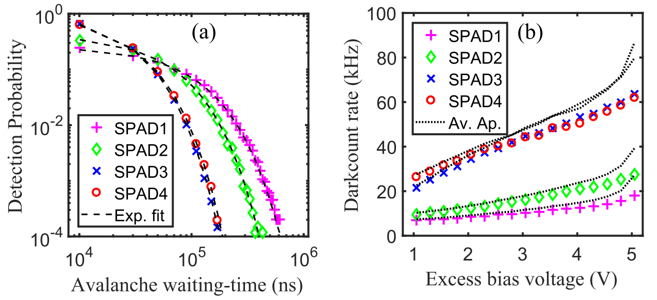

Fig. 4. (a) Measured results and exponential fitting of avalanche detection probabilities for $V_{ex} \simeq 4$ V and equal time bins of 2×10^4 ns. (b) Measured dark-count rate as a function of the applied excess bias voltage. Dotted lines: approximation based on average time intervals.

Furthermore, the average time between dark-count-based avalanche events is more than three orders of magnitude longer than the average afterpulsing time delay (see Fig. 3). Therefore, even when the afterpulsing probability is very high and it dominates the number of detections in dark noise statistics, the timing properties are nevertheless determined by the dark-count mechanism. It can be shown that even when a dark-count-based avalanche is followed by 10 afterpulses in average (supposing a Bernoulli process, this corresponds to an afterpulsing probability of $\sim$ 90%, which is quite high and impractical for receiver application), the proposed characterization method can still estimate the dark-count rates up to a few megahertz accurately. In fact, if we conduct an experiment based on randomly selected t_0 as explained before, a random time instant will most probably fall within a time interval corresponding to a dark-count waiting time and, thus, will leave the afterpulsing effect aside and is able to characterize the dark-count distribution with a very good approximation. In the following, it is shown how using this concept a similar experiment is performed to characterize other parasitic effects.

Using this experiment, the dark-count detection probabilities are estimated for different waiting times as shown in Fig. 4(a). The measurement results for all SPADs exhibit an excellent match to an exponential distribution (with a fitted time constant τ_{dc} inversely proportional to the corresponding dark-count rate, i.e., $r_{dc} = 1/\tau_{dc}$) demonstrating that the memorylessness assumption is realistic. Fig. 4(b) shows the obtained dark-count rates for all SPADs as a function of the applied excess bias voltage. Here, the dotted lines indicate that the dark-count rates are simply approximated as one over the average time intervals between successive detections including afterpulsing avalanche events. Such an approximation is good only at low excess bias voltages where the afterpulsing probability is small. However, at higher voltages, the number of avalanches fired by afterpulsing becomes larger, and thus, the overestimation of r_{dc} is more significant.

B. Afterpulsing and Crosstalk Measurement

The characterization of afterpulsing and crosstalk in a multi-SPAD structure is not an easy task due to their similar time delay regimes which are in the nanosecond range and close to our measurement's time resolution. In fact, one cannot simply consider only the avalanche detections in different SPADs which coincide within the same sampling time window as crosstalk. It is shown in the following that the "prompt" crosstalk has a negligible contribution as compared to the "delayed" crosstalk and this leads to an underestimation of crosstalk. Furthermore, if we suppose larger coincidence windows (e.g., 40–10 ns), then it can be shown that there is a relatively high chance that in different SPADs, we detect afterpulsing-based avalanches close in time, where only an initial simultaneous firing was created by crosstalk. This leads to an overestimation of crosstalk as all crosstalk- and afterpulsing-based avalanches are assumed as crosstalk-based events.

In order to overcome the above-mentioned difficulties and to avoid more complexities for providing electrical or optical access to SPADs solely, we apply the memorylessness concept again in a nanosecond regime. As it was described before, the dark-count mechanism dominates the timing properties of the dark noise statistics even when other mechanisms possess a higher quantity of detections. Therefore, any experiment characterizing the waiting time between a random instant and the first upcoming detection will be most probably terminated by a dark count even when other mechanisms dominate quantitatively. On the other hand, according to the memorylessness property, the distribution does not depend on the selected instant to measure the waiting time. Accordingly, the probability to detect an avalanche in an interval (e.g., Δt) can be obtained based on the exponential distribution corresponding to the dark-count mechanism and the memorylessness property as

$$\begin{aligned} P(t_0 < t^* < t_0 + \Delta t) &= 1 - P(t^* > t_0 + \Delta t \mid t^* > t_0) \\ &= 1 - P(t^* > \Delta t) \\ &= 1 - \int_{\Delta t}^{\infty} \frac{e^{-t/\tau_{dc}}}{\tau_{dc}} dt \\ &= 1 - e^{-\Delta t/\tau_{dc}} \end{aligned} \quad (2)$$

where t^* denotes the avalanche instant and t_0 is a randomly selected instant. For nanosecond-range intervals (e.g., $\Delta t = 2$ ns), we have $\Delta t \ll \tau_{dc}$, and thus, (2) can be approximated as

$$P(t_0 < t^* < t_0 + \Delta t) \simeq 1 - \left(1 - \frac{\Delta t}{\tau_{dc}}\right) = \frac{\Delta t}{\tau_{dc}}. \quad (3)$$

In order to characterize the afterpulsing and crosstalk, we designed the following experiment. First, values are drawn randomly for t_0 over the time between the first and the last recorded avalanche for each SPAD and then observe if an avalanche is recorded within the next 50× bins all having a width of 2 ns. Then, we repeat this observation for 10^6 times to estimate the detection probabilities by dividing the number of detection times by 10^6 corresponding to each time bin. According to (3), we expect small detection probabilities as the width of time bins are 4 to 5 orders of magnitude shorter than the dark-count time constant τ_{dc}. Fig. 5 presents the measurement results for SPAD 1 and SPAD 2 (specified by "Random t_0" on the plot) which fit well to the values predicted by (3). Now, we conduct a similar experiment but

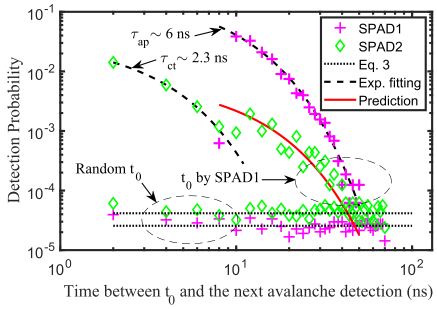

Fig. 5. Waiting-time distribution based on the interarrival and the random-to-arrival schemes. The data are obtained from SPAD 1 and SPAD 2 at $V_{ex} \simeq 4$ V.

instead of selecting t_0 randomly, we set t_0 as instants with the following feature. In the four-time sequences, we determine all detection instants that there has been no detection in all SPADs for the last 100 ns before them. This will guarantee that the afterpulsing and crosstalk effects have diminished and by firing an avalanche at t_0, the other SPADs are ready to fire a crosstalk-based avalanche and if fired, it will not be an afterpulse. Then, by dividing the number of detections by the total number of such t_0 instants, the probabilities corresponding to different time bins are obtained.

Fig. 5 shows such probabilities for SPAD 1 and SPAD 2, when t_0 is set to the detection instants in SPAD 1 with the above-mentioned feature. It is striking that the detection probabilities are increased significantly as compared to those of the experiment with random selection. The amount of increase regarding the time bins in SPAD 2 accurately characterizes the crosstalk in the first 9 ns (equal to the quencher dead time), as there is no chance for an afterpulsing in SPAD 1. After 9 ns, there is a chance for an afterpulsing-based avalanche in SPAD 1, which can be also accurately characterized by the amount of increase in the detection probabilities regarding the time bins in SPAD 1. Both the crosstalk (shown for SPAD 1-to-2 in Fig. 5) and the afterpulsing (shown for SPAD 1 in Fig. 5) exhibit a very good match to exponential distributions with time constants of $\tau_{ct} \simeq 2.3$ ns and $\tau_{ap} \simeq 6$ ns, respectively.

Now, we come to the point where the dead time can be estimated finer than the oscilloscope's resolution limit measuring the minimum time interval between subsequent avalanche detections. In fact, due to the time characteristics of the afterpulsing described by an exponential distribution (with $\tau_{ap} \simeq 6$ ns), we expect an average afterpulsing delay of 6 ns for an extremely short ($\simeq 0$) dead time. However, our measurements show that the average afterpulsing delay is $\simeq 15$ ns (at $V_{ex} \simeq 4$ V), which proves that the dead time is $\simeq 15 - 6 \simeq 9$ ns. In fact, according to the memorylessness of its distribution (1), if 9 ns has elapsed already (one dead time), the average waiting time afterward would still be $\tau_{ap} \simeq 6$ ns and, therefore, the total average waiting time would be equal to 15 ns.

It is reassuring to note that as the afterpulses in SPAD 1 can trigger crosstalk avalanches in SPAD 2, the detection probabilities in SPAD 2 show a second rising trend after the dead time in SPAD 1 (9 ns), which shows an acceptable fit to a prediction based on the multiplication of the obtained exponential fits for crosstalk in SPAD 1 and afterpulsing in SPAD 2 (shown by the solid line in Fig. 5).

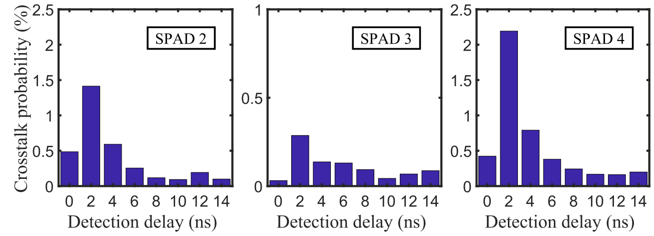

Fig. 6. Measured SPAD-to-SPAD crosstalk probabilities from SPAD 1 to the other SPADs for different delay values at $V_{ex} \simeq 4$ V. The time steps are equal to the time resolution of 2 ns.

Using the above-described experiment, the crosstalk between all SPADs can also be characterized based on one dark noise measurement. Fig. 6 shows the crosstalk probabilities from SPAD 1 to all other SPADs for the first 8-time bins after an avalanche. As it was expected, the crosstalk probability from SPAD 1 to its nonconsecutive SPAD (SPAD 3) is very small as compared to the neighboring SPADs. Furthermore, it is important to note that the prompt crosstalk has a negligible share of the total crosstalk as it is included only in the first time bin. In fact, a prompt crosstalk is triggered only when a photon is absorbed inside or very close to the depleted volume of another SPAD. This has a much smaller chance as compared to an absorption in the bulk. Therefore, the major part of crosstalk shows an average waiting time (delay) of about 3 ns, which we believe is caused by diffusion of optically generated carriers in the bulk. One should note that for the SPADs here, which are implemented in 0.35-μm PIN-photodiode CMOS technology, the drift time is in subnanosecond range [4]. However, the diffusion from substrate is considerably higher as compared to the thin SPADs based on P+/N-well structure.

IV. Results and Discussion

In this section, we consider the performance limitations imposed by different SPAD parasitics in an optical receiver. The error probabilities are investigated in single-SPAD and multi-SPAD structures and it is shown how the minimum necessary number of SPADs in a receiver array can be obtained.

A. Single-SPAD Receiver

The measurement results regarding the total afterpulsing probability and the average afterpulsing waiting time for all SPADs in the array as a function of the excess bias voltage are shown in Fig. 7(a). It indicates that for excess bias voltages higher than ~4 V, the afterpulsing probability increases exponentially. According to experimental investigations [4], the receiver shows the best BER for V_{ex} around 4 V, where the detection efficiency is high enough but the parasitics are still manageable. The average waiting time at this voltage is around 15 ns as shown in Fig. 7(b). This is higher than the fitted time constant of 6 ns obtained in Fig. 5. This is due to

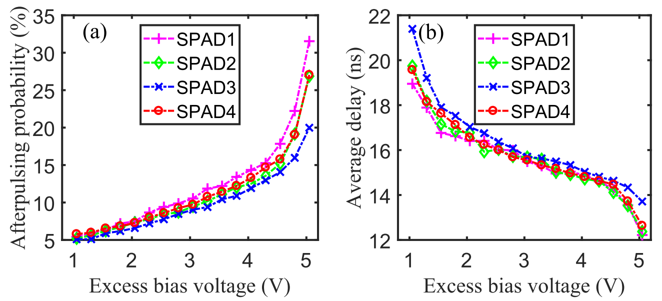

Fig. 7. (a) Measured afterpulsing detection probability and (b) waiting time as a function of the excess bias voltage. The detector dead time is ∼ 9 ns.

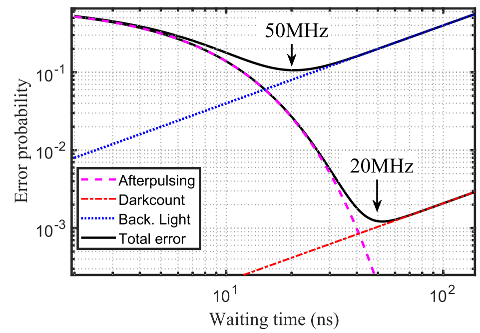

Fig. 8. Error probabilities for a logical "0" bit as a function of time for a single-SPAD receiver.

the dead time duration (∼ 9 ns), in which the SPAD is not recovered yet and cannot detect an afterpulse.

In order to gain insight into the effect of parasitics on the BER of the SPAD-based receivers, we investigate the performance of a single-SPAD structure based on the SPADs characterized earlier and a degree of freedom on the quencher dead time to determine the minimum possible parasitic effects.

Suppose that a logical "0" is obtained only when no avalanche is detected during the corresponding bit time. This means that any detection during a bit time is decided as a logical "1" and implicitly defines the fastest operating mode. In fact, it is limited to a single dead time as compared to a decision-making scheme, where there is a photon (detection) counting threshold of more than one. In such a single-SPAD receiver, the intrinsic parasitics are dark count and afterpulsing. Any avalanche caused by these mechanisms results in an error when a logical "0" has to be detected. Fig. 8 shows the sum of their probabilities indicated as total error regarding logical "0" bits as a function of time. According to (3), it is clear that the probability of a false detection due to the dark count increases linearly with the waiting time (i.e., the bit time). On the other hand, according to the experimental results shown in Fig. 5, the afterpulsing probability can be decreased exponentially if the SPAD reset is delayed after an avalanche. Assuming such flexibility, Fig. 8 demonstrates that the error probability due to intrinsic parasitics can be minimized to $\sim 10^{-3}$ for 50 ns (i.e., 20 MHz) operating frequency.

Unfortunately, this is not the whole story because one cannot neglect extrinsic parasitics (i.e., background light) in an optical receiver. Therefore, supposing a background light of about 80 photons per microsecond at a total photon detection efficiency of 5%, a total error including both intrinsic and extrinsic parasitics is also plotted in Fig. 8, which is around 0.1–0.2 for 50–100-MHz operating frequency (bit times of 10–20 ns). The background light rate of 80 photons per microsecond represents a realistic value equivalent to an optical power of 5 nW and an extinction ratio of 200 in accordance with the measured values in our experimental setup. This result indicates that, in practice, the single-SPAD receiver cannot achieve satisfactory performance solely. Therefore, in order to achieve smaller BER values, a multi-SPAD structure is required to reduce the parasitic effects. In fact, as these parasitics can be considered as stochastically independent random errors in different SPADs, the minimum achievable error probability regarding a "0" can be approximated as p_{err}^n, where n denotes the number of SPADs and p_{err}^n is the minimum error probability of a single SPAD. This corresponds to a decision rule, which decides for a logical "1" when all n SPADs in the receiver trigger an avalanche during the corresponding bit time. However, the multi-SPAD structure encounters an extra source of parasitics due to crosstalk. According to Fig. 8, with $n_{\mathrm{s}} = 4$ SPADs, the best achievable BER at 50–100-MHz operating frequency (without considering the crosstalk effect) can be estimated as $0.1^{n_{\mathrm{s}}}$-$0.2^{n_{\mathrm{s}}}$, which would be between 10^{-4} and 10^{-3}. The term n_{s} implicitly assumes that error happens in the receiver when an error is made in all SPADs simultaneously. This prediction shows a good agreement with the measured results in [4], where crosstalk does not degrade the performance significantly, and a BER of $\sim 10^{-3}$ is obtained at 50 MHz using four SPADs.

B. Crosstalk in Multi-SPAD Receiver

In order to study the effect of crosstalk on the BER of a multi-SPAD receiver, it is important to not only obtain the SPAD-to-SPAD (one-to-one) crosstalk probabilities but also to acquire an understanding of the receiver behavior in different conditions, i.e., the probability of firing i SPADs by crosstalk when j SPADs are already fired by any other mechanism ($p_{\mathrm{cr}}(i|j)$).

First, we define $\tilde{p}_{\mathrm{cr}}$ as the average all one-to-one crosstalk probabilities, which are obtained as explained in the previous section (see Figs. 5 and 6). The average one-to-one crosstalk probability and waiting time (delay) are summarized in Fig. 9(a) as a function of excess bias voltage V_{ex}. The average crosstalk increases with V_{ex}, as is expected. The crosstalk delay, however, shows a decrease in lower voltages but an increase above 4.5 V. We think that the increased crosstalk delay at higher V_{ex} is due to the increased probability of diffusing charge carrier from farther distances into the SPAD's depletion and multiplication region. In other words, the triggering probability regarding the carriers at closer distances may reach a saturation at $V_{\mathrm{ex}} \simeq 4$ V, while it still increases with V_{ex} for farther carriers.

In order to model the conditional crosstalk probabilities ($P_{\mathrm{cr}}(i|j)$), we assume that crosstalk is a Bernoulli process with the probability of $\tilde{p}_{\mathrm{cr}}$ $(1 - \tilde{p}_{\mathrm{cr}})$ to trigger an (no) avalanche in any available SPAD [21], [22]. Accordingly, for example in an

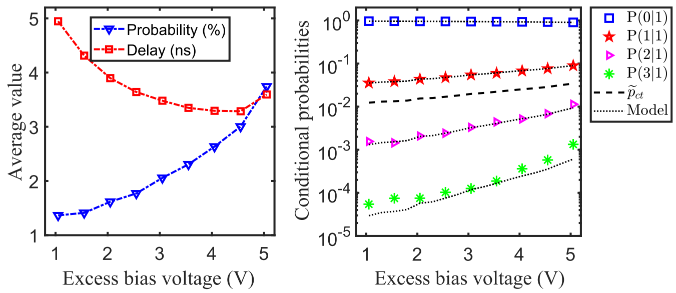

Fig. 9. (a) SPAD-to-SPAD crosstalk probability and delay. (b) Measured and model-predicted conditional crosstalk probabilities as a function of V_{ex}.

array of four SPADs, $P_{\mathrm{cr}}(0|1)$ representing the probability of firing $i = 0$ crosstalks when initially $j = 1$ SPAD is triggered, can be obtained by

$$P_{\mathrm{cr}}(0|1) = (1 - \tilde{p}_{\mathrm{cr}})^3 \tag{4}$$

as none of the three available SPADs should detect a crosstalk.

Furthermore, we include cascading processes [22], where a crosstalk-triggered avalanche may trigger the following avalanche in another available SPAD in the array. Therefore, as another example $P_{\mathrm{cr}}(1|1)$ representing the probability of firing one crosstalk ($i = 1$) when initially one SPAD ($j = 1$) is triggered can be obtained as

$$P_{\mathrm{cr}}(1|1) = 3\tilde{p}_{\mathrm{cr}}(1 - \tilde{p}_{\mathrm{cr}})^2(1 - \tilde{p}_{\mathrm{cr}})^2 \tag{5}$$

where the coefficient 3 stands for the number of available SPADs and the last term is due to the cascading process, where none of the other two available SPADs are fired by the third SPAD which has detected a crosstalk. In a similar manner, $P_{\mathrm{cr}}(i|j)$ can be obtained for other possible combinations of i and j as

$$\begin{aligned}
P_{\mathrm{cr}}(2|1) &= 3\tilde{p}_{\mathrm{cr}}^2(1 - \tilde{p}_{\mathrm{cr}})^3 + 6\tilde{p}_{\mathrm{cr}}^2(1 - \tilde{p}_{\mathrm{cr}})^4\\
P_{\mathrm{cr}}(3|1) &= \tilde{p}_{\mathrm{cr}}^3 + 3\tilde{p}_{\mathrm{cr}}^2(1 - \tilde{p}_{\mathrm{cr}})\big(1 - (1 - \tilde{p}_{\mathrm{cr}})^2\big)\\
&\quad + 3\tilde{p}_{\mathrm{cr}}(1 - \tilde{p}_{\mathrm{cr}})^2\big(\tilde{p}_{\mathrm{cr}}^2 + 2\tilde{p}_{\mathrm{cr}}^2(1 - \tilde{p}_{\mathrm{cr}})\big)\\
P_{\mathrm{cr}}(0|2) &= (1 - \tilde{p}_{\mathrm{cr}})^4\\
P_{\mathrm{cr}}(1|2) &= 2\big(1 - (1 - \tilde{p}_{\mathrm{cr}})^2\big)(1 - \tilde{p}_{\mathrm{cr}})^3\\
P_{\mathrm{cr}}(2|2) &= \big(2\tilde{p}_{\mathrm{cr}} - \tilde{p}_{\mathrm{cr}}^2\big)^2\\
&\quad + 2\big(2\ \tilde{p}_{\mathrm{cr}} - \tilde{p}_{\mathrm{cr}}^2\big)\tilde{p}_{\mathrm{cr}}(1 - \tilde{p}_{\mathrm{cr}})^2\\
P_{\mathrm{cr}}(0|3) &= (1 - \tilde{p}_{\mathrm{cr}})^3\\
P_{\mathrm{cr}}(1|3) &= 1 - (1 - \tilde{p}_{\mathrm{cr}})^3.
\end{aligned} \tag{6}$$

It is clear that for a given j, the sum of all probabilities over different i values must be equal to one. This can be simply verified for $j = 1, 2,$ and 3 by inspection of (4)–(6).

In order to evaluate the above-described modeling of $P_{\mathrm{cr}}(i|j)$, we measured the corresponding values using our experimental dark noise data. The obtained $P_{\mathrm{cr}}(i|j)$ values for $j = 1$ are averaged over all SPADs as initializing (triggering) SPAD and are plotted in Fig. 9(b) (indicated by dotted lines) for different i values. It is worth mentioning that in order to take the cascading process within the measurements into account, the next 8 ns after each avalanche detection has been considered and if the following avalanche is detected, it is counted as a (cascading) crosstalk. According to Fig. 9(b), the results show an excellent agreement between the direct measurement of conditional crosstalk probabilities and model predictions based on the measured $\tilde{p}_{\mathrm{cr}}$ and (4)–(6).

V. Conclusion

A statistical investigation of the intrinsic parasitic effects in multi-SPAD optical receivers is presented. The characterization method is implemented based on the dark noise statistics, which are straightforward to measure. The simple but crucial memoryless nature of the dark noise statistics is the key for understanding and identifying the parasitic effects. Probabilities and timing characteristics of different parasitics are obtained at different excess bias voltages. The results are used to model conditional crosstalk behavior, and our next step is to use these obtained results for modeling the BER of the optical receiver. This will enable us to evaluate the contribution of different parasitics to the BER and to identify the bottlenecks for further optimizations.

References

[1] J. A. Richardson, E. A. G. Webster, L. A. Grant, and R. K. Henderson, "Scaleable single-photon avalanche diode structures in nanometer CMOS technology," *IEEE Trans. Electron Devices*, vol. 58, no. 7, pp. 2028–2035, Jul. 2011, doi: 10.1109/TED.2011.2141138.

[2] E. Fisher, I. Underwood, and R. Henderson, "A reconfigurable single-photon-counting integrating receiver for optical communications," *IEEE J. Solid-State Circuits*, vol. 48, no. 7, pp. 1638–1650, Jul. 2013, doi: 10.1109/JSSC.2013.2253222.

[3] D. Chitnis and S. Collins, "A SPAD-based photon detecting system for optical communications," *J. Lightw. Technol.*, vol. 32, no. 10, pp. 2028–2034, May 15, 2014, doi: 10.1109/JLT.2014.2316972.

[4] H. Zimmermann, B. Steindl, M. Hofbauer, and R. Enne, "Integrated fiber optical receiver reducing the gap to the quantum limit," *Sci. Rep.*, vol. 7, no. 1, 2017, Art. no. 2652, doi: 10.1038/s41598-017-02870-2.

[5] S. Cova, M. Ghioni, A. Lacaita, C. Samori, and F. Zappa, "Avalanche photodiodes and quenching circuits for single-photon detection," *Appl. Opt.*, vol. 35, no. 12, pp. 1956–1976, 1996, doi: 10.1364/AO.35.001956.

[6] M. Ghioni, A. Gulinatti, I. Rech, F. Zappa, and S. Cova, "Progress in silicon single-photon avalanche diodes," *IEEE J. Sel. Topics Quantum Electron.*, vol. 13, no. 4, pp. 852–862, Jul./Aug. 2007, doi: 10.1109/JSTQE.2007.902088.

[7] H. Zimmermann, *Integrated Silicon Optoelectronics*, 2nd ed. Berlin, Germany: Springer, 2010, doi: 10.1007/978-3-642-01521-2.

[8] D. P. Palubiak and M. J. Deen, "CMOS SPADs: Design issues and research challenges for detectors, circuits, and arrays," *IEEE J. Sel. Topics Quantum Electron.*, vol. 20, no. 6, Nov./Dec. 2014, Art. no. 6000718, doi: 10.1109/JSTQE.2014.2344034.

[9] L. Zhang *et al.*, "A comparison of APD- and SPAD-based receivers for visible light communications," *J. Lightw. Technol.*, vol. 36, no. 12, pp. 2435–2442, Jun. 15, 2018, doi: 10.1109/JLT.2018.2811180.

[10] E. Sarbazi, M. Safari, and H. Haas, "Statistical modeling of single-photon avalanche diode receivers for optical wireless communications," *IEEE Trans. Commun.*, vol. 66, no. 9, pp. 4043–4058, Sep. 2018, doi: 10.1109/TCOMM.2018.2822815.

[11] E. Sciacca *et al.*, "Crosstalk characterization in geiger-mode avalanche photodiode arrays," *IEEE Electron Device Lett.*, vol. 29, no. 3, pp. 218–220, Mar. 2008, doi: 10.1109/LED.2007.915373.

[12] A. Vacheret *et al.*, "Characterization and simulation of the response of multi-pixel photon counters to low light levels," *Nucl. Instrum. Methods Phys. Res. A, Accel. Spectrom. Detect. Assoc. Equip.*, vol. 656, no. 1, pp. 69–83, 2011, doi: 10.1016/j.nima.2011.07.022.

[13] D. A. Kalashnikov, S.-H. Tan, and L. A. Krivitsky, "Crosstalk calibration of multi-pixel photon counters using coherent states," *Opt. Express*, vol. 20, no. 5, pp. 5044–5051, 2012, doi: 10.1364/OE.20.005044.

[14] A. Gallivanoni, I. Rech, and M. Ghioni, "Progress in quenching circuits for single photon avalanche diodes," *IEEE Trans. Nucl. Sci.*, vol. 57, no. 6, pp. 3815–3826, Dec. 2010, doi: 10.1109/TNS.2010.2074213.

[15] R. Enne, B. Steindl, M. Hofbauer, and H. Zimmermann, "Fast cascoded quenching circuit for decreasing afterpulsing effects in 0.35-μm CMOS," *IEEE Solid-State Circuits Lett.*, vol. 1, no. 3, pp. 62–65, Mar. 2018, doi: 10.1109/LSSC.2018.2827881.

[16] S. Cova, A. Lacaita, and G. Ripamonti, "Trapping phenomena in avalanche photodiodes on nanosecond scale," *IEEE Electron Device Lett.*, vol. 12, no. 12, pp. 685–687, Dec. 1991, doi: 10.1109/55.116955.

[17] A. W. Ziarkash, S. K. Joshi, M. Stipčević, and R. Ursin, "Comparative study of afterpulsing behavior and models in single photon counting avalanche photo diode detectors," *Sci. Rep.*, vol. 8, no. 1, Mar. 2018, Art. no. 5076, doi: 10.1038/s41598-018-23398-z.

[18] I. Rech *et al.*, "Optical crosstalk in single photon avalanche diode arrays: A new complete model," *Opt. Express*, vol. 16, no. 12, pp. 8381–8394, 2008, doi: 10.1364/OE.16.008381.

[19] S. Jahromi and J. Kostamovaara, "Timing and probability of crosstalk in a dense CMOS SPAD array in pulsed TOF applications," *Opt. Express*, vol. 26, no. 16, pp. 20622–20632, 2018, doi: 10.1364/OE.26.020622.

[20] E. Sciacca *et al.*, "Silicon planar technology for single-photon optical detectors," *IEEE Trans. Electron Devices*, vol. 50, no. 4, pp. 918–925, Apr. 2003, doi: 10.1109/TED.2003.812095.

[21] M. Ramilli, A. Allevi, V. Chmill, M. Bondani, M. Caccia, and A. Andreoni, "Photon-number statistics with silicon photomultipliers," *J. Opt. Soc. Amer. B, Opt. Phys.*, vol. 27, no. 5, pp. 852–862, 2010, doi: 10.1364/JOSAB.27.000852.

[22] L. Gallego, J. Rosado, F. Blanco, and F. Arqueros, "Modeling crosstalk in silicon photomultipliers," *J. Instrum.*, vol. 8, no. 5, p. P05010, 2013, doi: 10.1088/1748-0221/8/05/P05010.

Hiwa Mahmoudi received the M.Sc. and Ph.D. degrees from the Sharif University of Technology, Tehran, Iran, and the Vienna University of Technology, Vienna, Austria, in 2009 and 2014, respectively.

Since 2014, he has been with the Institute of Electrodynamics Microwave and Circuit Engineering, Vienna University of Technology, as a Post-Doctoral Researcher, focusing on simulation and analysis of integrated circuits.

Michael Hofbauer received the Dipl.Ing. degree in electrical engineering, and the Ph.D. degree from the Vienna University of Technology (TU Wien), Vienna, Austria, in 2011 and 2017, respectively, and the Ph.D. degree (Hons.) Sub auspiciis Praesidentis.

Since 2005, he has been with the Institute of Electrodynamics Microwave and Circuit Engineering, TU Wien, where he became an University Assistant in 2016. He has authored and co-authored over 50 publications.

Bernhard Steindl received the Dipl.Ing. degree from the Vienna University of Technology, Vienna, Austria, in 2013, where he is currently pursuing the Ph.D. degree with the Institute of Electrodynamics, Microwave and Circuit Engineering.

In 2011, he joined the Institute of Electrodynamics, Microwave and Circuit Engineering, Vienna University of Technology, doing his master thesis on characterization of APDs. He has authored and co-authored over 20 journal and conference papers. His research interests include optoelectronics, APDs, SPADs, and simulation of semiconductor devices.

Kerstin Schneider-Hornstein received the Dipl.Ing. and Dr.techn. degrees from the Vienna University of Technology, Vienna, Austria, in 2000 and 2004, respectively.

Since 2001, she has been with the Institute of Electrodynamics, Microwave and Circuit Engineering, Vienna University of Technology. She has authored the book *Highly Sensitive Optical Receivers* (Springer, 2006), and the author and co-author of over 50 journal and conference papers.

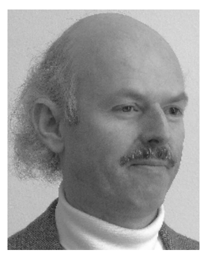

Horst Zimmermann (SM'02) received the Dr.Ing. degree from Duke University, Durham, U.K., in 1991.

He was an Alexander-von-Humboldt Research-Fellow at Duke University, working on diffusion in Si, GaAs, and InP. In 1993, he joined Kiel University, Kiel, Germany, working on optoelectronic integration. Since 2000, he has been a Full Professor in circuit engineering with the Vienna University of Technology, working on (Bi)CMOS analog and optoelectronic full-custom design.